Thermooptical molecule sieve on the microscale

Natan Osterman[1] and Dieter Braun[2]
[1)] *Department of Complex Matter, J. Stefan Institute, Jamova 39, 1000 Ljubljana, Slovenia,*
[2)] *Systems Biophysics, Physics Department, Center for Nanoscience, Ludwig-Maximilians-Universität München, Amalienstrasse 54, 80799 Munich, Germany*

A combination of thermophoresis and fluid flow can be used to trap molecules and particles. We show that heating by scanning motion of an elongated laser spot creates a strong thermal trap. Additionally, it induces a global fluid flow that feeds the trap. Such "thermal sieve" can accumulate molecules from a large surrounding region within seconds into a 10 μm spot. Numerical modeling gives a quantitative prediction of the effect. Traps can be dynamically created, relocated and tuned, which can be used for particle sorting.

One of the long-standing goals of science and technology is a contact-free manipulation of small particles. While it is possible to trap atoms in vacuum using magnetic traps, thermal noise is much stronger when particles are under biological conditions, i.e. in water at room temperature. Optical tweezers can manipulate particles larger than about 500 nm whereas for smaller particles and molecules, typically strong electrical fields are used. Electrophoresis is well developed technique but lacks flexibility since it needs sophisticated electrode-barrier geometries. Also, in water it does not discriminate between molecule sizes and gel electrophoresis has to be applied. A less used principle for micro-manipulation is thermophoresis[1–6] where molecules are moved by a thermal gradient. Strong thermal gradients can be generated by laser heating, bringing the flexibility and microscale definition of a contact-less all-optical approach.

Thermophoresis typically depletes molecules away from hot areas[7,8]. In order to confine the molecules in a small region the effect has to be combined with a fluid flow. The simplest realization is a flow directed against the thermal gradient, where the molecules are trapped upstream of the warm spot[9]. The accumulation can be amplified in elongated columns by thermal convection flow[10,11] or in flat geometries where toroidal convection flow yields point accumulations[12,13]. The molecules are pushed by thermophoresis into one side of the flow and are transported preferentially in one direction. This leads to a strong accumulation in a confined region, which is then called a thermal trap. However, the molecules have to enter the trap by diffusion, limiting the accumulation kinetics.

Fluid flows can be created optothermally by thermoviscous pumping[14,15]. A combination of a thermal gradient across the chamber and bidirectional flow creates a micro "conveyor belt" where molecules are preferentially transported in one direction. Multiple conveyors arranged in a toroidal geometry generate an effective molecule trap[16], but it is inherently unstable and therefore useless in practical applications.

Here we demonstrate a simple yet very effective optothermal molecule trap. Scanning motion of an elongated laser spot on an absorbing surface of a thin microfluidic chamber creates a thermal gradient perpendicular to the surfaces and gives rise to a circulating convection-like fluid flow. The superposition of both processes creates a thermal molecule trap which strongly accumulates colloidal particles and biomolecules. Additionally, the laser scanning induces a global fluid flow which feeds the trap with surrounding particles and overcomes the diffusion limitation. Like an ordinary sieve separates and accumulates wanted elements from unwanted material, our *thermal sieve* depletes molecules from a large surrounding region and accumulates them within seconds. Similarly to other optothermal molecule trap designs, the approach does not require microfluidics, electrodes, biochemical or local inhomogeneous surface modifications and can be thus dynamically created and relocated. The use of multiple thermal sieves enables a host of interesting applications, most prominently particle sorting. We show accumulation and spatial separation of a binary colloidal mixture with a sequence of two sieves.

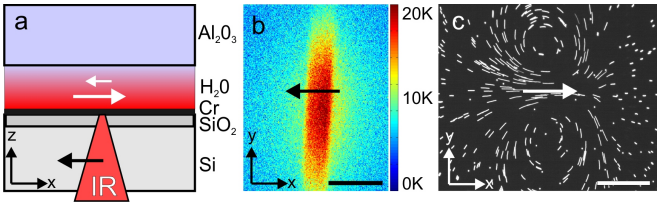

Figure 1. Experimental setup and basic properties of a thermal sieve. (a) Chamber cross-section. A liquid is sandwiched between chromium coated silicon bottom and a top sapphire window. An elliptically deformed IR laser beam is absorbed in the Cr layer thus creating an elongated hot spot. Scanning motion of the laser in the negative x-direction creates a fluid flow (white arrows) in the positive x-direction close to the bottom and a weak backflow close to the top surface. An additional effect is a temperature gradient in z-direction. (b) Fluid temperature increase when the laser is scanning over the 50 μm wide region. (c) Flow visualized by 1 μm fluorescent tracers. Scale bar in all micrographs is 100 μm.

Experimental setup. A 10 μm thin fluid layer is sandwiched between a bottom oxidized silicon wafer and a top 170 μm thick sapphire window (Fig. 1a) to enhance thermal gradients. The silicon wafer (thickness 0.5 mm, polished on both sides, 1 μm SiO_2, MEMC Electronic Materials Inc.) is coated on one side with a 100 nm chromium layer by vacuum evaporation. A collimated IR

laser beam (RLD-5-1455, IPG Photonics, $\lambda = 1455$nm, 5 W) is deflected with a scanning mirror (6200-XY, Cambridge Technology), guided through a cylindrical lens (f=100 mm) and then finally focused onto a sample with a long working distance lens (f = 40 mm) resulting in an elliptically shaped laser spot. The laser passes through the Si wafer which is transparent to the IR light but heats the Cr layer by absorption. The focus is being scanned typically over a 50 μm long line with a kHz repetition frequency, resulting in a scanning speed of 50 mm/s. The movement is unidirectional, i.e. the laser is turned off when returning back to the starting position. The dimensions of the hot spot are 18 μm in the direction of scanning and 260 μm in the perpendicular direction.

Imaging is realized with a fluorescence microscope (Axiotech Vario, Zeiss; 20x air objective) using a cyan LED for illumination (Luxeon V Star) and a CCD camera (pco.1400, PCO Imaging). Temperature imaging is provided with a temperature dependent fluorescence dye BCECF (100 μM in 10 mM TRIS-HCl buffer, Invitrogen), 150 ms after switching on the laser heating and normalized against a previously taken cold picture[17]. The temperature response of the dye was calibrated in a separate measurement in the same chamber under external temperature control. The temperature increase when the laser focus is being scanned over a 50 μm long line along the x-axis is 20K (Fig. 1b). The sapphire window has a high thermal conductivity and cools the fluid sheet, resulting in a temperature gradient in the z-direction. The evidence for the steep gradient is rapid movement of 1 μm beads from the hot bottom to the top cold chamber surface when the laser is turned on.

The unidirectional scanning of the hot spot across the chamber pumps the fluid. It is the result of a broken symmetry between thermal expansion and contraction in the front and the wake of the hot spot due to temperature dependent viscosity[14]. Flow was tracked with 1 μm fluorescent polystyrene beads (F8888, Invitrogen) immediately after the laser was switched on (Fig. 1c). To analyze it in more detail we separately filled the same chamber with 500 nm beads in a 50% glycerol - 50% 1 mM TRIS buffer mixture. Bead diffusion was strongly suppressed which enabled us to image non-disturbed flow trajectories.

Beads near the bottom surface of the chamber rapidly travel against the direction of the laser scanning with velocities of up to 180 μm/s whereas beads near the upper chamber surface travel in the opposite direction with up to 40 μm/s (Video 1 in[18]). Such a vertical velocity gradient is easy to understand. The temperature increase in the hot spot is falling with the increasing height above the bottom absorbing layer. Optothermal pumping scales quadratically with the peak temperature of the moving temperature spot. Consequently the liquid moves faster at the bottom. The reason for the backflow close to the upper surface is the conservation of mass. Due to the opposing fluid pressure outside of the scanning region it is energetically more favorable to position a part of a backflow in the pumping region rather than to have only

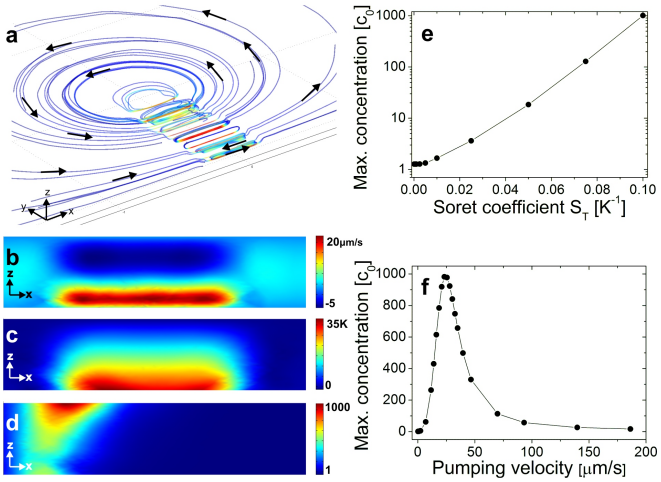

Figure 2. Finite element simulation of a thermal sieve. The long axis of the hot spot is oriented in y-direction and is being scanned in the negative x-direction. a) Isometric view of a few flow trajectories. Thermo-viscous pumping results in a fast circular convection-like flow in the pumping region and a global, slower flow outside. Arrows mark the direction of the flow. (b, c, d) Central 70μm $\times$ 5μm cross-section (not in scale) at $y = 0$ of (b) the x-component of the flow velocity, (c) temperature increase and (d) molecular concentration. (e) Maximum sieve accumulation exponentially increases with the Soret coefficient S_T. f) Dependence of the accumulation on the fluid pumping velocity for $S_T = 0.1$/K and $D = 10\mu\text{m}^2$/s, typical values for 300 bp DNA or 100 nm polystyrene beads.

backflows at the sides. The superposition of the flow and the backflow in the pumping region leads to a bidirectional, circular convection-like flow pattern which is a necessary condition for a thermal trap. The surrounding large scale flow outside of the pumping region which is bringing new matter overcomes the diffusion limit and thus leads to a very efficient thermal trap.

Numerical modeling. We simulated the 3D Navier-Stokes equation of the flow field using a finite element solver (Comsol, FEMLAB). Since the problem is symmetric with the respect to the direction of the pumping (xz-plane) only a half of the experimental chamber was simulated. The simulation box $500 \times 500 \times 5\,\mu\text{m}^3$ was much larger than the scanning region to probe the fluid dynamics around the trap. A general isometric view of the simulated flow trajectories is presented in Fig. 2a. There are two distinct flow regimes: a fast circular convection-like roll emerges in the scanning region while outside the flow is much slower. The flow trajectories extend through all available volume and end in the central roll. As shown in Fig. 2b, the liquid travels in the pumping direction near the chamber bottom and in the opposite direction near the top surface. The flow outside of the scanning region is unidirectional with the typical parabolic shape of the Poisseuile flow. The results of the simulation closely match the experimentally observed flow of Fig. 1c.

To model the trapping, the temperature was included in the simulation. It is calculated from boundary conditions which are set to match the experimentally observed temperature gradient. The highest temperature is reached in the laser absorbing layer at the bottom chamber surface. The dissipated heat is transported away through the silicon bottom and upper sapphire window, resulting in a thermal gradient in z-direction (Fig. 2c). Knowing the flow field v and the temperature T, the concentration distribution c can be simulated. The equation for the particle mass flow j in the case of low concentrations ($c \ll 1$) reads[19]

$$j = vc - D\left(S_T c\left(1-c\right)\nabla T - \nabla c\right).$$

It consists of a flow transport term, a thermophoretic term and a diffusive term. D is the diffusion coefficient and $S_T = D_T/D$ the Soret coefficient of the particles. As shown in Fig. 2d, the molecules accumulate near the top (cold) chamber surface. Similarly to the other thermal trap designs[10,16,17] the accumulation exponentially depends on the temperature increase and S_T , as shown in Fig. 2e. By changing the laser power, the temperature gradient is varied and thus the trap efficiency can be adjusted. We will show later how this principle can be exploited to separate particles. For a given S_T there exists an optimal pumping velocity which enables the best accumulation (Fig. 2f). At lower than optimal pumping velocities the diffusion smears out the confinement of molecules while at higher velocities the molecules do not have enough time to thermophoretically migrate from the hot to the cold side of the circular convection-like flow. The optimal velocity for a few micrometer thin chamber is on the order of $100\,\mu$m/s, easily achievable using thermo-viscous pumping.

Another important parameter for the trapping efficiency is the aspect ratio of the central pumping area. The maximum achievable concentration exponentially depends on the ratio between the sieve size and the chamber thickness[17].

Accumulation. We have accumulated various kinds of colloidal particles and molecules to experimentally demonstrate the flexibility and trapping efficiency of the thermal sieve. In Fig. 3 we present the accumulation of DNA molecules. For 22-base single-stranded DNA in 1 mM TRIS buffer a steady state accumulation of 5-fold was reached within 6 s after the laser was turned on (Video 2 in[18]). When the laser was turned off we observed free diffusion into the environment which is a clear indication that the molecules had not adsorbed to the surface during the process of accumulation. As predicted by time-dependent FEM simulation and confirmed experimentally, the thermal sieve was able to accumulate the short DNA fragments merely 5-fold due to the high diffusion coefficient $\left(D = 180\,\mu\text{m}^2/\text{s}\right)$. Conversely, long DNA molecules can be trapped much better as demonstrated by the accumulation of 5.8 kbp double-stranded DNA in 1 mM TRIS where a 60-fold increase of concentration is reached within seconds.

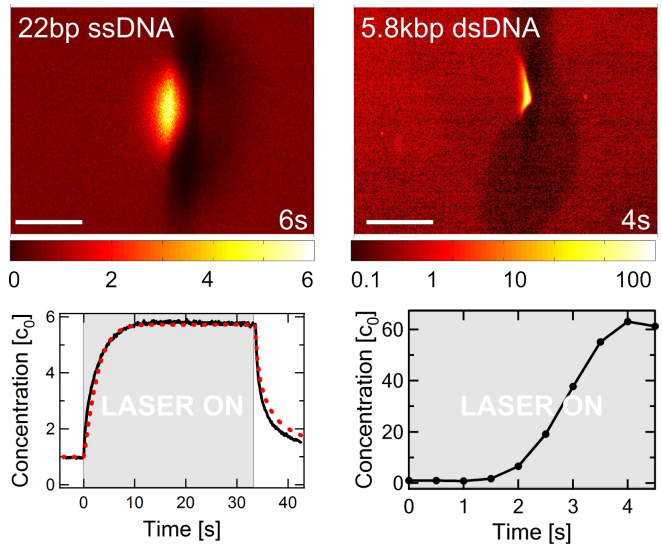

Figure 3. Accumulation of DNA molecules. *Left:* Short 22-base ssDNA is accumulated 5-fold within 6 s. The chart shows the concentration in the center of the trap. The simulation (red dotted line) matches the experiment. *Right:* 5.8-kbp dsDNA is accumulated 60-fold in 4 s. Scale bar in both micrographs is $100\,\mu$m.

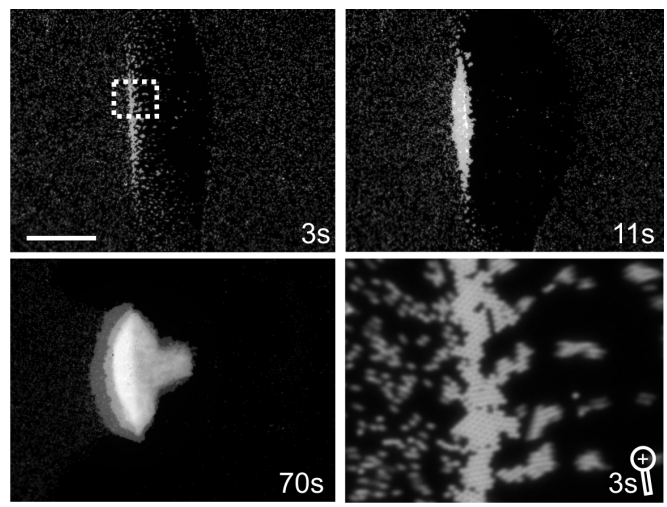

Figure 4. Accumulation of $1\,\mu$m beads. (a) A 2D colloidal crystal is formed[13] in 3 s. A global fluid flow causes rapid accumulation: within 10 s a second crystal layer starts to emerge. All beads from a $400 \times 400\mu\text{m}^2$ surroundings are accumulated in 70 s. Scale bar is $100\,\mu$m. (b) Magnified image at 3 s.

Colloidal particles are even easier to trap due to their low diffusion, $D = 0.5\,\mu\text{m}^2/\text{s}$, and high $S_T = 10/\text{K}$. Fig. 4 shows the accumulation in a dilute solution of $2a = 1\,\mu$m polystyrene beads in 1mM TRIS. When the laser is turned on, the temperature gradient is strong enough such that the particles that are in the scanning region ballistically move to the cold chamber surface (Peclet number $Pe > 1$). The global fluid flow feeds the

trap and within 3 s a two-dimensional colloidal crystal is formed at the inflow border of the scanning region. The mutually attractive interparticle force that gives rise to crystallization is a consequence of a thermophoretic slip flow[13,20] which is observed when the thermal gradient exceeds $(a \cdot S_T)^{-1}$. After 10 s, the bottom layer is packed closely and a second crystal layer starts to emerge. All particles from a wider area around the trap are accumulated after one minute in a closely packed 3-layer colloidal crystal of $100 \times 100\,\mu\text{m}^2$ size.

Sorting. As a hallmark application of the thermal sieve we demonstrate particle sorting based on the thermophoretic response of particles. Traditionally, particles are separated using thermal field flow fractionation[21,22] where long channels in combination with low flow rates and high temperature differences are needed to establish a high separation ratio. Kinetics of separation is typically on the hours time scale. Oppositely, at microscopic scale large temperature gradients can be created with application of small temperature differences which is especially beneficial for biological samples. Micro-thermal field-flow fractionation was used for particle size distribution analysis[23] or thermophoretic separation[24,25]. Maeda et al.[26] demonstrated trapping and separation of solutes like DNA, RNA and colloids in solution of polyethylene glycol (PEG) by using laser heating. The driving force of the separation was chemical contrast between solutes and PEG. Our approach is based on a fluid-dynamical and thermophoretic contrast, while adding PEG would provide an additional modulation of the trapping.

Particle separation is achieved in two steps: particles of all kinds are first accumulated using a strong thermal sieve, then two (or more) thermal sieves with increasing trapping efficiencies are created in series along the pumping direction. Fig. 5 displays the sorting of a dilute suspension of 200 nm and $1\,\mu$m fluorescent beads. A strong sieve was used to accumulate both kinds of beads for 48 s. To begin the separation, the strong sieve was turned off and two other sieves were created, one weaker, $70\,\mu$m, and one stronger, $140\,\mu$m away. Large beads (with high S_T) immediately got trapped in the weak sieve while a large portion of the small beads (with small S_T) passed through it and was caught in the strong sieve. To quantify the sorting process, the fluorescence was averaged over $20\,\mu\text{m}^2$ areas at the sieve positions as indicated by the white arrows in Fig. 5. The chart of fluorescence vs. time reveals the time dynamics of the spatial separation process. One might note that the fluorescence of sieve 2 is higher than that of sieve 1 which is due to the additional particles accumulated from the surroundings when sieve 1 was already turned off.

Conclusion. We have presented a way to accumulate molecules and particles using an optically generated thermal sieve. A simple laser scanning simultaneously creates a thermal trap and induces a fluid flow on a much larger scale which feeds the trap. The accumulation is therefore not limited by slow diffusion of particles as in other thermal trapping designs. We demonstrated the speed and high trapping efficiency by accumulating colloidal particles and DNA molecules. The all-optical creation of thermal sieves allows their dynamic creation, relocation and change of their strength. Since trapping efficiency exponentially depends on S_T it is possible to tune the trap to certain types of particles. We proved the principle with a spatial separation of a binary colloidal mixture. In contrast to separation in an optical lattice[27], our mechanism does not need external fluid flow. FEM simulation reproduced the experimental findings remarkably well. The simulation also allows analysis and optimization of more complex systems such as series of thermal sieves in a microfluidic chip.

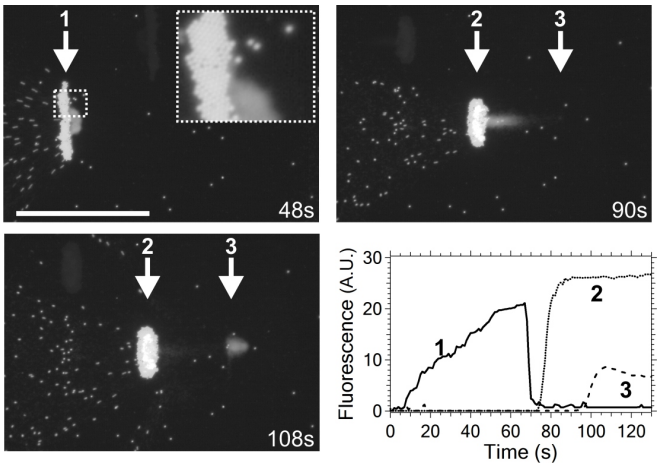

Figure 5. Spatial separation of a mixture consisting of 200 nm and $1\,\mu$m beads (Video 3 in[18]). A strong thermal sieve (its location is denoted with arrow 1) is first used to accumulate beads. As shown in the inset, large beads crystallize whereas the accumulated small beads appear as a bright spot at the right side. To separate them, sieve 1 is switched off and one weaker (arrow 2) and one stronger (arrow 3) sieve are created. Large beads accumulate in the weak sieve while small beads pass through and accumulate in the strong sieve. The chart shows fluorescence at the positions of sieves 1, 2, 3 versus time after the first sieve was turned on. Scale bar is $100\,\mu$m.

The found thermal sieve is suited to accumulate, sort and fractionate molecules and particles within integrated microfluidic systems, and can be applied in colloidal, molecular and biological research. For example, thermal sieves can be used to enhance diffusion-limited reactions, actively route molecules and accumulate them close to detector for improved detection sensitivity, such as amplifying small binding signals in probing the affinity of biomolecules in microscale thermophoresis. Given the flexibility and ease of implementation we anticipate that the thermal sieve could be widely used as a functional block in a host of applications.

We acknowledge financial support from the NanoSystems Initiative Munich, the ERC Starting Grant, and grants no. J1-6724 and P1-0192 from the Slovenian Research Agency.

REFERENCES

[1] C. Soret, Arch. Sci. Phys. Nat. Geneve **2**, 48 (1879).
[2] S. Duhr and D. Braun, Physical Review Letters **96**, 168301 (2006).
[3] H.-R. Jiang, H. Wada, N. Yoshinaga, and M. Sano, Physical Review Letters **102**, 208301 (2009).
[4] G. Mcnab, Journal of Colloid and Interface Science **44**, 339 (1973).
[5] R. Piazza, Journal of Physics: Condensed Matter **16**, S4195 (2004).
[6] S. A. Seidel, P. M. Dijkman, W. A. Lea, G. van den Bogaart, M. Jerabek-Willemsen, A. Lazic, J. S. Joseph, P. Srinivasan, P. Baaske, A. Simeonov, I. Katritch, F. A. Melo, J. E. Ladbury, G. Schreiber, A. Watts, D. Braun, and S. Duhr, Methods **59**, 301 (2013).
[7] S. Duhr and D. Braun, Proceedings of the National Academy of Sciences **103**, 19678 (2006).
[8] R. Piazza and A. Guarino, Physical Review Letters **88**, 208302 (2002).
[9] S. Duhr and D. Braun, Physical Review Letters **97**, 038103 (2006).
[10] P. Baaske, F. M. Weinert, S. Duhr, K. H. Lemke, M. J. Russell, and D. Braun, Proceedings of the National Academy of Sciences **104**, 9346 (2007).
[11] K. Clusius and G. Dickel, Naturwissenschaften **26**, 546 (1938).
[12] D. Braun and A. Libchaber, Physical Review Letters **89**, 188103 (2002).
[13] S. Duhr and D. Braun, Applied Physics Letters **86**, 131921 (2005).
[14] F. M. Weinert and D. Braun, Journal of Applied Physics **104**, 104701 (2008).
[15] F. Weinert, J. Kraus, T. Franosch, and D. Braun, Physical Review Letters **100**, 164501 (2008).
[16] F. M. Weinert and D. Braun, Nano Letters **9**, 4264 (2009).
[17] C. B. Mast and D. Braun, Physical Review Letters **104**, 188102 (2010).
[18] See supplementary material at [URL will be inserted by AIP] for the experimental videos.
[19] S. Wiegand, Journal of Physics: Condensed Matter **16**, R357 (2004).
[20] R. Di Leonardo, F. Ianni, and G. Ruocco, Langmuir **25**, 4247 (2009).
[21] T. Squires and S. Quake, Reviews of Modern Physics **77**, 977 (2005).
[22] J. C. Giddings, M. Martin, and M. N. Myers, Separation Science and Technology **14**, 611 (1979).
[23] J. Janča, J.-F. Berneron, and R. Boutin, Journal of Colloid and Interface Science **260**, 317 (2003).
[24] P. Geelhoed, R. Lindken, and J. Westerweel, Chemical Engineering Research and Design **84**, 370 (2006).
[25] D. Vigolo, R. Rusconi, H. A. Stone, and R. Piazza, Soft Matter **6**, 3489 (2010).
[26] Y. Maeda, A. Buguin, and A. Libchaber, Physical Review Letters **107**, 038301 (2011).
[27] M. P. MacDonald, G. C. Spalding, and K. Dholakia, Nature **426**, 421 (2003).